TOWARD THE OPTIMAL RESOLUTION OF RAINFALL ESTIMATES TO OBTAIN RELIABLE URBAN HYDROLOGICAL RESPONSE: X-BAND POLARIMETRIC RADAR ESTIMATES APPLIED TO ROTTERDAM URBAN DRAINAGE SYSTEM

Ricardo Reinoso-Rondinel[1] *, Guendalina Bruni[2], Marie-Claire ten Veldhuis[2] and Herman Russchenberg[1]

[1] Department of Geoscience and Remote Sensing, Delft University of Technology, Delft, Netherlands
[2] Water Management Department, Delft University of Technology, Delft, Netherlands

Abstract

Weather observations are conventionally performed by single polarization C-band weather radars with a temporal and spatial resolution of 5 min and 1 km, respectively. However, for urbanized areas, these spatial and temporal resolutions may not be sufficient to detect, monitor, and obtain accurate rainfall rate estimates of fast-evolving weather phenomena. In this work, a S-band vertical profiler (TARA) and a X-band horizontal scanner polarimetric weather radars (IDRA) located in the Cabauw Experimental Site for Atmospheric Research (CESAR) observatory are used to characterize physical processes and obtain accurate rainfall rate estimates of severe thunderstorms at high temporal and spatial resolutions. A large convective front over Western Europe on January 03 2012 was observed by the C-band operational radar from The Royal Netherlands Meteorological Institute (KNMI in Dutch initials) and by both, IDRA and TARA. It is expected the new insights will be revealed based on the polarimetric and the high-resolution capabilities from both radars. Moreover, rainfall rate estimates obtained from IDRA are used to simulate rainfall at lower spatial resolutions to analyze the spatial rain variability over a simulated urban drainage system belonging to Rotterdam urban area.

1. INTRODUCTION

The operational KNMI weather radar network in the Netherlands consists of two C-band Doppler radars. Both radars are used to obtain quality precipitation estimation (QPE) with a resolution of 2.5 by 2.5 km every 5 min. For in-situ measurements, the operational rain gauge network consists of 330 gauges with a temporal resolution of 1 day (Schuurmans et al., 2007). However, for urbanized areas, these spatial and temporal resolutions may not be sufficient to detect, monitor, and obtain accurate rainfall rate estimates of fast-evolving weather phenomena (Schellart et al., 2012). It is also known that, due to land use characteristics of urban areas and also to the small scale of urban catchments (i.e., few hectares up to few square kilometers), it is not uncommon that the time lag between rainfall and runoff peaks is of the order of few minutes. Therefore, finer weather observations at urban scales are needed.

In this context, X-band radars are widely used to obtain QPE at higher spatial and temporal resolutions. For example, the research Center for Collaborative Adaptive Sensing of the Atmosphere (CASA) consists of a network of X-band radars that can adaptively scan the regions with rapidly-evolving weather (Brotzge et al., 2005). In Japan, the National Research Institute of Earth Science and Disaster Prevention (NIED) had established a X-band dual polarization radar network (X-NET) in Metropolitan Tokyo area (Maki et al., 2010). In Western Europe, the RainGain project includes a network of X-band radars to obtain high resolution QPE in urbanized cities to cope with urban flood and to reduce flooding damage (http://www.raingain.eu). The main advantages of using X-band radars for weather observations at urban scales are: a) they do not require big antennas to transmit fine beams achieving high antenna rotation speeds, and b) high spatial resolution can be obtained by setting reasonably short coverage range for urban scales. The main disadvantage of weather X-band radars is that, transmitted and received signals can be highly attenuated by regions with heavy precipitation; and therefore, decreasing the capability to detect regions far away from the radar.

In this work, a long-lived convective front over Western Europe is observed and analyzed at distinct spatial and temporal resolutions to assess the variability of heavy precipitation at urban scales. In section 2, infrared satellite observations are shown to identify low and high clouds. High resolution weather observations are presented in section 3 to obtain physical information of the convective front. In section 4, the variability of

---

* *Corresponding author address:* Ricardo Reinoso-Rondinel, Delft University of Technology, Department of Geoscience and Remote Sensing, Stevinweg 1, Room 02.120.B2, Delft, 2628 CN, Netherlands; e-mail: r.r.reinosorondinel@tudelft.nl

QPE at urban scales is shown. Finally, a summary and conclusions are given in section 5.

2. WEATHER SATELLITE OBSERVATIONS

Infrared (IR) satellites are used to measure cloud temperatures and IR satellites images are typically shown in gray scale; e.g., cooled clouds are shown as white. Knowing the temperature of clouds, cold and warm fronts can be distinguished (Ahrens, 2012). Cold fronts are associated with cold and vertical development clouds, e.g., cumulus clouds. Lifting of clouds occurs along fronts; i.e., between distinct air masses and convective long lines of thunderstorms can develop along frontal boundaries; i.e., frontal squall lines. Warm fronts are linked with stratiform clouds producing stratiform precipitation over a large area, commonly, in front of the warm front. In this work, a large weather convective system over the North Sea of Europe was observed on January 03 2012 by the IR satellite SAT24-EISQ51 as shown in Figure 1. Panel a) shows group of clouds at 1200 UTC with a cyclone located on the North Sea moving eastward. It can be distinguished two groups of clouds, one extended group and one narrowed located east and south of the cyclone, respectively. This may indicate that a warm front is followed by a cold front. In order to better distinguish both fronts, the pressure surface analysis map at 1200 UTC is shown in panel b). Here, the low pressure (T) is in the center of the cyclone with two associated fronts where the warm front is followed by a cold front approaching the cost of The Netherlands, driven by the low and high pressure systems. Panel c) shows the cold front passing through The Netherlands at 1500 UTC. It is know that cold fronts trigger cloud vertical development and can produce severe squall lines or individual storm cells (Lamb and Verlinde, 2011). The next section will be focused on convective weather observations over The Netherlands collected by weather radars at different spatial and temporal resolutions.

3. WEATHER RADAR OBSERVATIONS

In contrast to the synoptic scale observed by SAT24-EISQ51, the same convective system was observed by weather radars. In general, weather radars cover smaller areas than satellites but with higher spatial and temporal resolutions. One of the most fundamentals weather radar products is the so-called reflectivity (Z). Reflectivity is related to signal power and depends on the number of hydrometeors per unit volume, size, physical state, and shape of hydrometeors (Doviak and Zrnić, 1993). In this work, three radars located in the Dutch

province of Utrecht, the operational radar installed in DeBilt and two research radars, IDRA and TARA, in Cabauw (Leijnse et al., 2010) will be used.

3.1. DeBilt Radar Observations (C-band)

The operational radar installed in DeBilt, hereafter De-Bilt radar, is a horizontal polarized and pulsed radar operating at C-band frequency of 5.6 GHz (Beekuis and Holleman, 2008). It has a maximum range of 320 km with a range resolution of 1 km and it coverages a volumetric region every 5 min by rotating the antenna 360° in azimuth and tilting the antenna in elevation from 0.3° to 25°. The weather system shown in Figure 1 is now analyzed by the DeBilt radar. A long lived squall line was identified by the DeBilt radar from 1200 to 1600 UTC, approximately, as shown in Figure 2. The reflectivity field at elevation angle of 0.4° and centered at DeBilt province is shown in panel a) at 1400 UTC. Here, reflectivity values higher than 40 dBZ can be seen along the convective line approaching the cost of The Netherlands. Typically, a squall line is a line of convective storms that forms along the cold front with a predominately trailing stratiform precipitation (Storm et al., 2007). However, due to the warm front previously discussed, the convective line show a leading and trailing stratiform precipitation. The evolution of the squall line is shown by panels b), c), and d), at 1430, 1500, and 1530 UTC, respectively. Note the multiple embedded bow echoes segments along the convective line through a) ... d).

In the literature review, squall lines also known as multicell line is associated with a moderate shear between 10 and 20 ms^{-1} and with strong updraft (Weisman and Rotunno, 2004). If winds increase rapidly with height ahead of a strong front, thunderstorms triggered along the boundary may organize into severe storms called supercell storms. For a localized analysis with a much higher spatial and temporal resolutions, IDRA observations are presented below.

3.2. IDRA Radar Observations (X-band)

IDRA is one of the research radars installed in CESAR observatory (i Ventura and Russchenberg, 2009) and it is 23 km southwest from DeBilt radar. IDRA is a frequency modulated continuous wave (FMCW) and dual-polarimetric radar working at X-band frequency of 9.475 GHz. The standard operational range is of 15 km with a range resolution of 30 m. It scans at a fixed elevation angle of 0.5° and rotates the antenna over 360° every 1
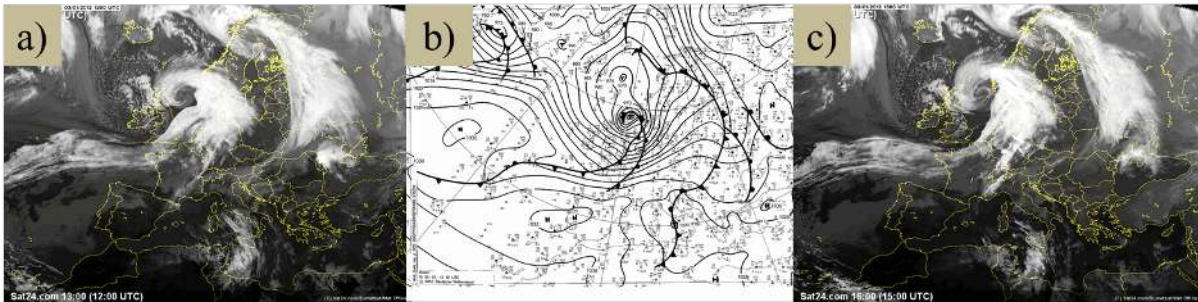
Figure 1: Panel a) shows an infrared (IR) satellite imagery from SAT24-EISQ51 over Europe on 1200 UTC, 03 January 2012 showing the strong frontal zone over the Netherlands associated with a deep low pressure system centered over the North Sea. Panel b) displays the corresponding synoptic chart at ground level, courtesy of the German Weather Service. Panel (c) is as in a) but 3 hours later at 1500 UTC, 03 January 2012.
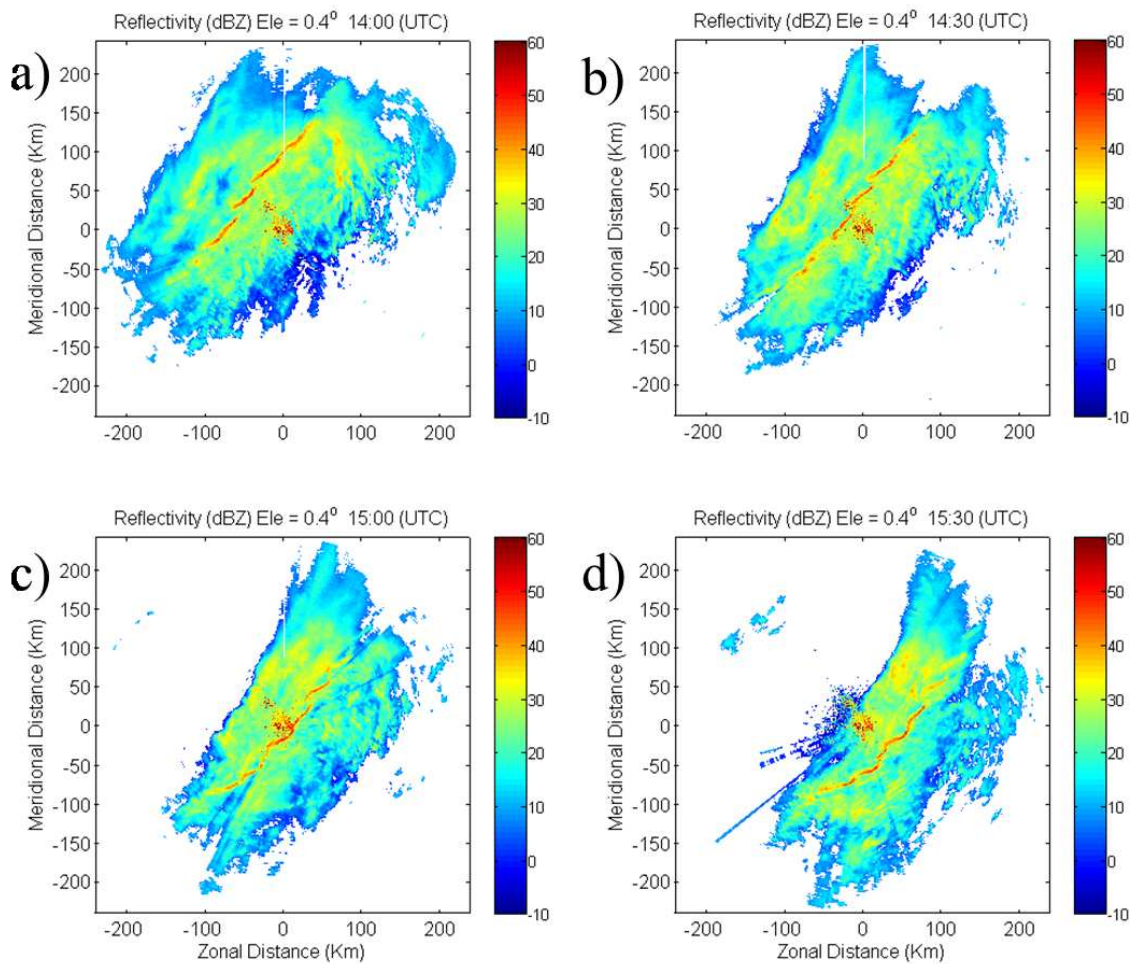

Figure 2: Reflectivity field at elevation angle of $0.40°$ observed by DeBilt radar. The evolution of the squall line from 1400 to 1530 UTC sampled at 30 min is shown in panels a) ... d). The squall line moves southeastward passing over DeBilt city. Note the large attenuated area northwest of DeBilt shown in panel d).
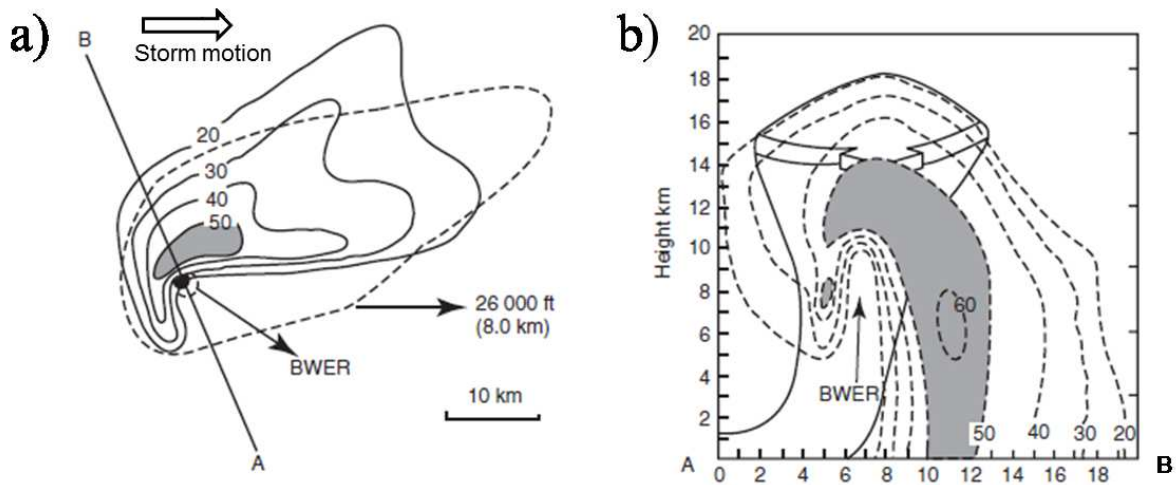
Figure 3: Schematic representation of a mature phased supercell storm. a) Top view: Contours lines at low-levels indicate reflectivity gradients from 20 to 50 dBZ. Note the hooklike echo and the bounded weak echo region (BWER) located at the southwest flank of the cell. b) Vertical cross-section view: Solid lines indicate the updraft and the outflow aloft. Reflectivity gradients from 20 to 60 dBZ are shown by dashed lines. The strong downdraft is shown by the gray area. The BWER is indicated by the vertical arrow located within the updraft region.
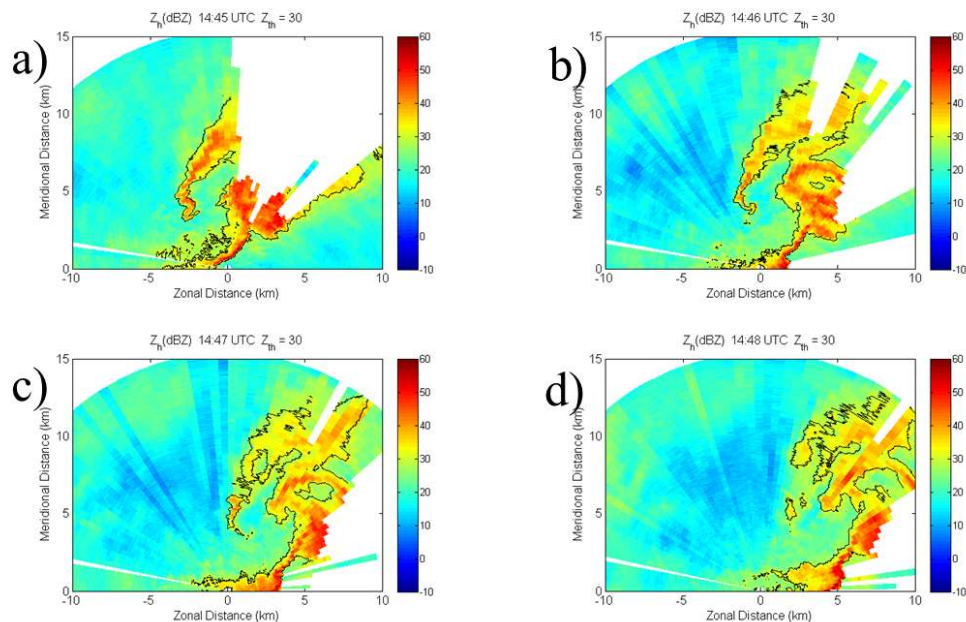

Figure 4: Reflectivity field observed by IDRA at elevation angle of 0.50°. The fast-evolve storm is shown by panels a) ... d) from 1445 to 1448 UTC. The 30 dBZ contour is denoted by the black line and regions inside the IDRA coverage with saturated received power are shown as black areas. Panel a) shows the hooklike echo on the southwest flank of the storm. Panel b) shows a storm with similar features to the schematic representation of a mature supercell storm shown in Figure 3. The early dissipation stage of the storm is shown by panels c) and d).
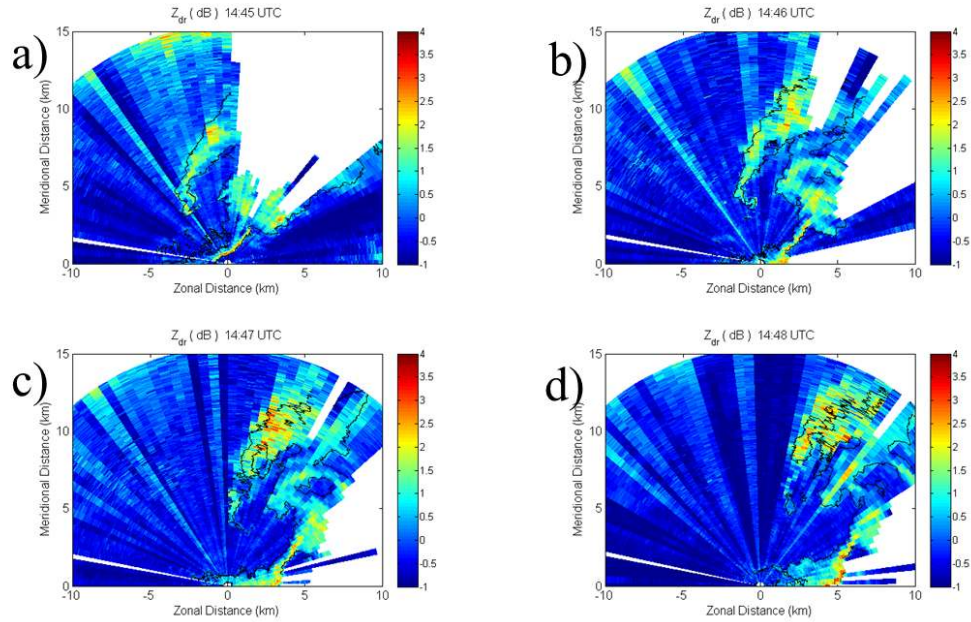
Figure 5: Differential reflectivity field observed by IDRA at elevation angle of 0.50°. Large oblate shaped drops are concentrated in the north flank of the storm. The hooklike echo shows the presence of medium oblate drops.
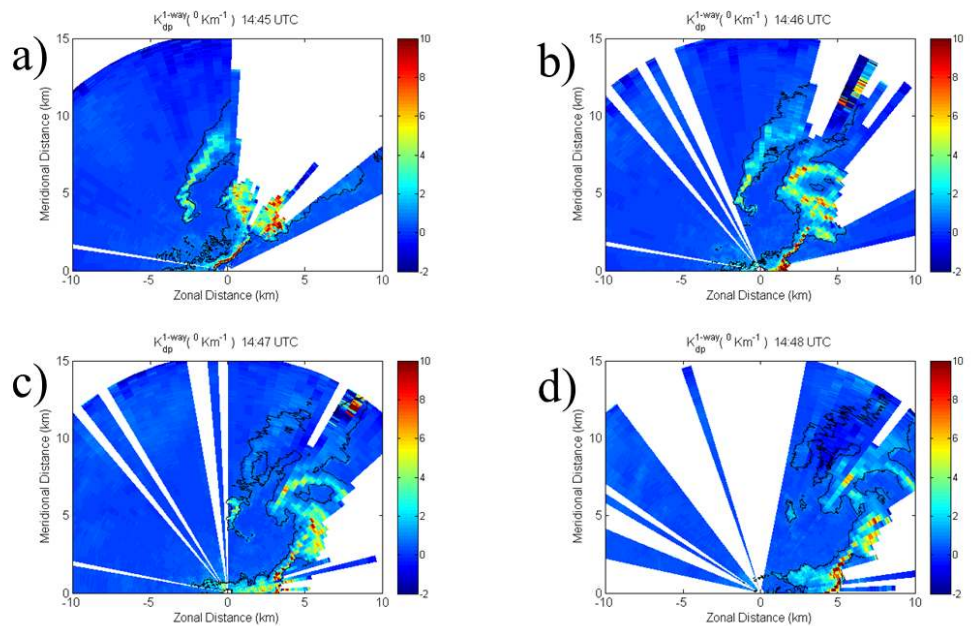

Figure 6: Specific differential phase field observed by IDRA at elevation angle of 0.50°. Areas with the largest differential phase are located over the hooklike echo and eye-shaped storm regions.

min. Observations obtained by IDRA were able to captured storm features associated with supercell storms but at much smaller scale. Therefore, a brief introduction to convective storm conceptual model is outlined next.

The initiation of suerpcell storms includes conditional instability, warm moist air, and source of lift. Typically, supercells are isolated, long lived of 5 hours, and are associated with strong shears larger than 20 m s^{-1}. But it can also be surrounded by other cells and short lived of 1 hour or less (Bunkers et al., 2006). The conceptual model on a mature stage supercell according to Weisman (2003) is shown in Figure 3. The horizontal cross-section at low-levels is shown in panel a). Reflectivity gradients from 20 to 50 dBZ are indicated by the solid contour lines. The reflectivity core is noted by the gray area. Note the hooklike appendage located at the southwest flank of the cell. The hooklike appendage or hook echo is the result of precipitation echoes around the rotating updraft. The area free of rain inside the hook echo is the bounded weak echo region (BWER) also associated with the updraft. BWER is bounded at sides and top by strong echoes. Panel b) shows a vertical cross-section of the supercell along the segment AB shown in panel a). The updraft and the outflow aloft are indicated by the solid countour line. The BWER is bounded by reflectivity echoes denoted by the dashed lines. The strongest downdraft is represented by the gray area with reflectivity larger than 50 dBZ. These mentioned signatures are described next using IDRA observations.

The reflectivity field sampled by IDRA from 1445 to 1448 UTC is shown in Figure 4. Panel a) shows strong reflectivity echoes moving eastward at 1445 UTC. Blank spots correspond to areas of received saturated power and 30 dBZ contours are denoted by black lines. Panel b) is similar to panel a) but at 1446 UTC. Here, the reflectivity field shows a very similar structure to the supercell storm model showed in Figure 3 a), but at much smaller scale. Both, the hooklike appendage and the BWER are clearly seen in the center of the reflectivity field; that is, the southwest flank of the storm cell. As mentioned above, the hooklike echo and the BWER are due to the rotating updraft carrying precipitation away. Another feature associated with the rotating updraft is given by the eye-shaped echo east of the hooklike echo. The small region free of rain in the center of the eye-shaped echo increases as shown in panels c) and d), at 1447 and 1448 UTC, respectively. Instead of a gradual strengthening of the hooklike storm cell, it dissipates rapidly. One hypothesis is that the eye-shaped storm cut the inflow which feeds the hooklike storm over the right forward flank and therefore weakening the dynamic source lifting (Bluestein, 2008). Two well known polarimetric variables, differential reflectivity (Z_{dr}) and specific dif-

ferential phase (K_{dp}), are discussed below (Bringi and Chandrasekar, 2001).

First, the differential reflectivity is defined as the ratio of reflectivities at the horizontal and vertical polarization. Z_{dr} does not depend on the number of hydrometeors as that is the case for reflectivity; instead, on the size and shape of hydrometeors. The Z_{dr} field is shown in Figure 5. Panel b) shows high values of Z_{dr}; i.e., large raindrops on the north side of the hooklike storm. On the other hand, the hooklike echo region contains small values of Z_{dr} and that is the region the initially dissipates as shown in panels c) and d). Second, the specific differential phase is the range derivative of the accumulated phase difference between the forward wave propagation in the horizontal and vertical directions. The K_{dp} field is shown in Figure 6. It can be seen that the hooklike echo region contains large values of K_{dp}; i.e., a large number of raindrops are concentrated in this region. However, the size of these raindrops should be small because Z_{dr} values are low in the hooklike region. K_{dp} field also shows the eye-shaped storm associated with a rotating updraft. In order to analyze the convective hooklike storm, data collected by TARA is presented next.

3.3. TARA Radar Observations (S-band)

The research profiler radar TARA is a FMCW dual polarized radar working at S-band frequencies of 3.3 GHz (Heijnen et al., 2000). TARA is able to obtain profiles from 200 m up to 38 km with a standard range resolution of 75 m. The temporal resolution of each profile is 1.5 sec and the elevation angle can be set manually between 0° and 90°. The hooklike storm cell will be described next by TARA based on reflectivity, linear depolarization ratio, radial velocity, and wind direction (Doviak and Zrnić, 1993).

Vertical profiles of the hooklike storm obtained at elevation angle of 75° are shown in Figure 7. The x-axis express the time from 1429 to 1500 UTC and the y-axis the range from 200 m to 4000 m. Panel a) shows the reflectivity field manifesting similar features to those from the supercell conceptual model shown in Figure 3 b) but at smaller scales. For example, the top of the storm cell is only 3 km, approximately, which is a much smaller version of the conceptual model. Nevertheless, the updraft-downdraft couple and the BWER can be seen around 1444 UTC, approximately. The downdraft core is noted by reflectivity values larger than 40 dBZ. In consequence, the melting layer breaks and after the storm leaves the TARA boresight, the melting layer begins to develop again from 1000 m and raise up to 1500 m.
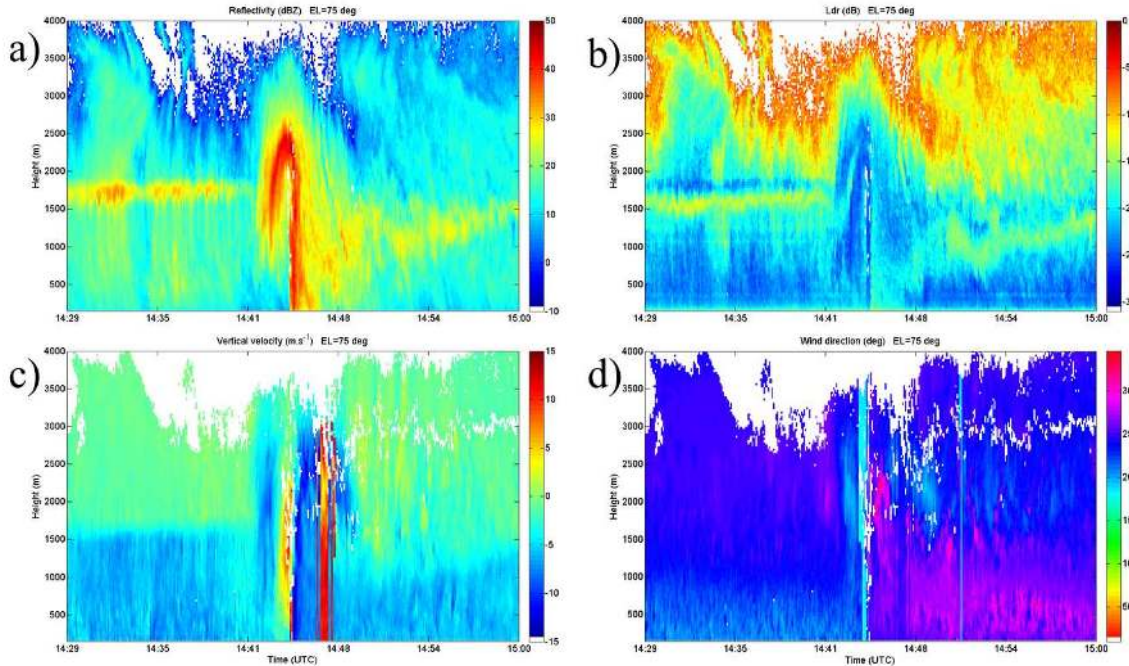
Figure 7: Height-time profile observations by TARA at elevation angle of 75°. The variables of reflectivity, linear depolarization ratio, vertical velocity, and wind direction are shown in panels a), b), c), and d), respectively, from 1429 to 1500 UTC. Storm profiles captured between 1441 and 1448 UTC, approximately, show high similarities to the vertical cross-section of a mature supercell storm shown in Figure 3

Panel b) shows the linear depolarization ratio (L_{dr}). L_{dr} is a measure of the ratio of the received vertical power to the transmitted horizontal signal or vice versa and it is a good indicator of mixed hydrometeors (Bringi and Chandrasekar, 2001). Downdraft regions show small L_{dr} values indicating pure rain. On the other hand, high values of L_{dr} can be related to the melting layer containing mixed hydrometeors. The radial velocity (v_r) is shown in panel d). Hydrometeors falling to the ground and those being lifted by the updraft are indicated by negative and positive v_r, respectively. Large hydrometeors falling to the ground are located in the main downdraft reaching negative velocities of 12 m s^{-1}, approximately. On the other hand, small hydrometeors being lifted by the updraft reach positives velocities of 10 m s^{-1}. Finally, panel d) shows the wind direction (w). At low levels, the cold front is notable by southwester winds, $w = 200^0$, lifting air masses coming from northwest, $w = 300^0$, respectively. The following section describes the rainfall variability in space and time over the simulated urban catchment of Rotterdam city.

4. TEMPORAL AND SPATIAL RAIN VARIABILITY

The focus of this section is to analyze the spatial variability of rainfall in time and space over a simulated catchment from the Rotterdam city (Bruni et al., 2013). Rainfall rate (R) was estimated based on differential phase measurement obtained by IDRA (Otto and Russchenberg, 2012). The estimated rainfall rate at 1446 UTC is shown in Figure 8. Only areas with R larger than 2 mm hr^{-1} are shown. At the first glance, the variability of R can be noted. For example, rainfall rate values smaller than 20 mm hr^{-1} are indicated by blue-tone colors. Values of rainfall rate between 20 and 50 mm hr^{-1} are given by green-tone colors. Those values can be seen within the hooklike echo and eye-shaped regions. Regions with rainfall rate values larger than 50 mm hr^{-1}, indicated by the red-tone colors, are found in the eye-shaped and south regions of the storm. The simulated catchment is denoted by the dashed rectangular with an area of 6 km^2, approximately. The location of the simulated catchment was chosen in a way that, the catchment received the largest amount of precipitation. The rain variability within the catchment is described next.

First, the rainfall field representation was mapped from polar to Cartesian coordinates resulting in squared grids
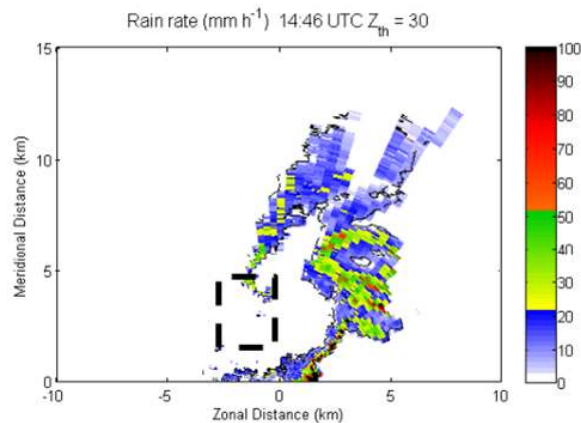
Figure 8: Estimated rainfall rate by IDRA at elevation angle of $0.50°$ and 1446 UTC. Note that heavy precipitation is located within the hooklike echo of the storm. The dashed black rectangular simulates the urban catchment in Rotterdam city.

of 100 m^2. Rainfall rate over the catchment area obtained by IDRA every 1 min is shown in Figure 9. At 1439 UTC, panel a), only light precipitation is observed. From 1440 to 1443 UTC, panels b) ... e), storm regions with rainfall rates larger than 20 mm hr^{-1} passed over the catchment. At 1444 UTC, panel f), the storm left the catchment area and only light precipitation is observed again. Note that the storm moves rapidly over 5 min, temporal variability, and the revisit time of operational radars is of 5 min. In consequence, storm revisit times of 5 min are not enough to capture this kind of fast-evolving storm. The spatial rainfall variability is explained below.

The rainfall rate map shown in panel c) of Figure 9 was used to simulate rainfall rate at lower spatial resolutions as shown in Figure 10. Squared grids of 100, 500, and 1000 m^2 are shown in panels a), b), and c), respectively. Figure 10 shows that if conventional radar; e.g., C-band radars, were used to estimate rainfall rates over urban scale catchments, the showed spatial rain variability will not be able to be captured.

Now, to analyze the rain variability over the urban catchment during the storm event, the accumulated rainfall depth in mm (A) was estimated. The accumulated rainfall depth for each grid of the catchment is the accumulated sum of rainfall depth over time. Examples of A sampled every 1 min from 1200 to 1530 UTC are shown in Figure 11. Three grids of 100 m^2 (p1, p2, and p3) located within one larger grid of 1000 m^2 (P) were chosen to asses rainfall spatial variability. A from grids p1, p2, p3, and P are shown by the red, blue, green, and thick black line colors, respectively. Before 1440 UTC, approximately, part of the leading stratiform precipitation

was over the catchment location; and therefore, A from the four grids are similar and smaller than 1 mm. However, when part of the convective line passes over the catchment site, from 1440 UTC approximately, A from the four grids reaches different values larger than 1mm.

5. SUMMARY AND CONCLUSIONS

Conventional weather radars usually coverage a large spatial domain but limited to obtain precipitation information at poor spatial and temporal resolutions. X-band radars are suitable for urban scale observations and possibly overcome such limitation. Rainfall rate of a fast-evolving storm was estimated to show spatial rain variability over an urban catchment area.

A convective squall line storm was used to test the capability of high resolution for the analysis of rain variability in time and space on the dual polarimetric IDRA. The variability of rain in time over the simulated urban catchment of Rotterdam city was evaluated by capturing snapshots of rainfall rate field over 5 min. For the spatial rain variability, rainfall rate obtained by IDRA and simulated rainfall rate at lower spatial resolutions were compared using the accumulated rainfall depth. In addition, high resolution weather observations were able to depict storm processes related to severe weather as shown by IDRA and TARA.

In summary, high resolution weather observation is vital for obtaining accurate rainfall rate estimates. As illustrated in this work, such X-band dual polarimetric IDRA should be used for weather observations at urban scale. It is foreseen that in such high resolution precipitation context, urban hydrology users will benefit from better description of fast runoff processes and short response times, leading to significant improvements on real-time urban flood forecasting.

References

Ahrens, C. D., 2012: *Meteorology Today: An Introduction to Weather, Climate, and the Environment*. Cengage Learning, Belmont, CA, USA, 10th edition.

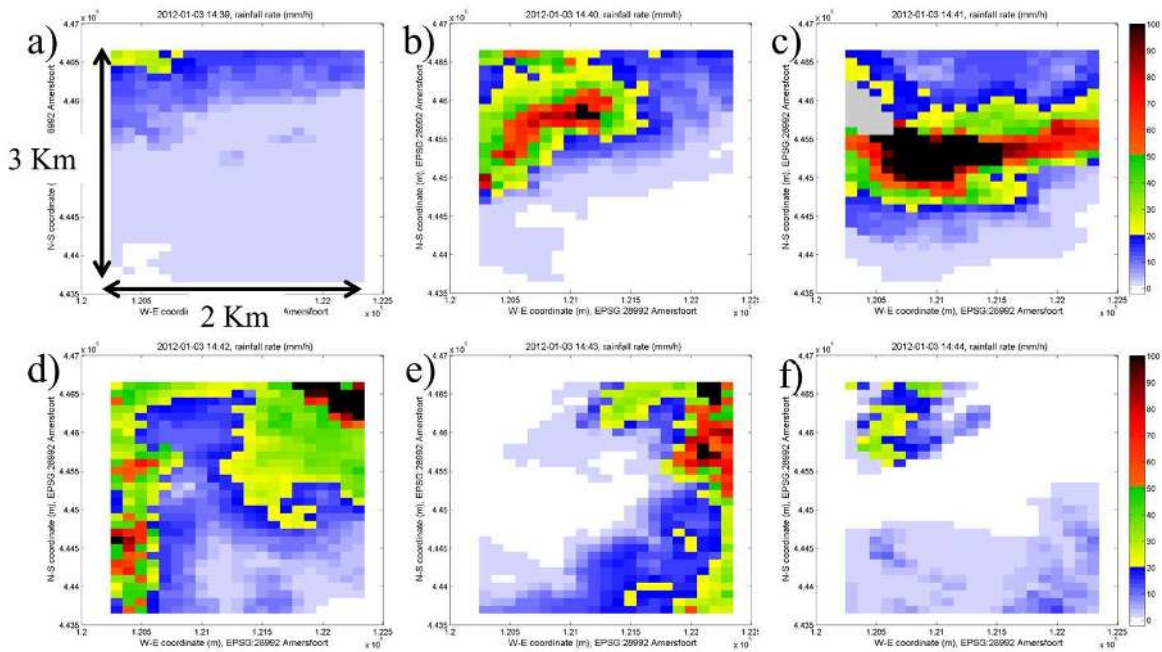Beekuis, H., and I. Holleman, 2008: From pulse to product: Highlights of the digital-IF upgrade of the dutch

Figure 9: Rainfall rate over the simulated urban catchment. Estimated rainfall rate from 1439 to 1444 UTC sampled every 1 min is shown by panels a) ... f). The catchment size is of 2 by 3 km, approximately, as shown in panel a). Grids were mapped to grids of 100 by 100 m.
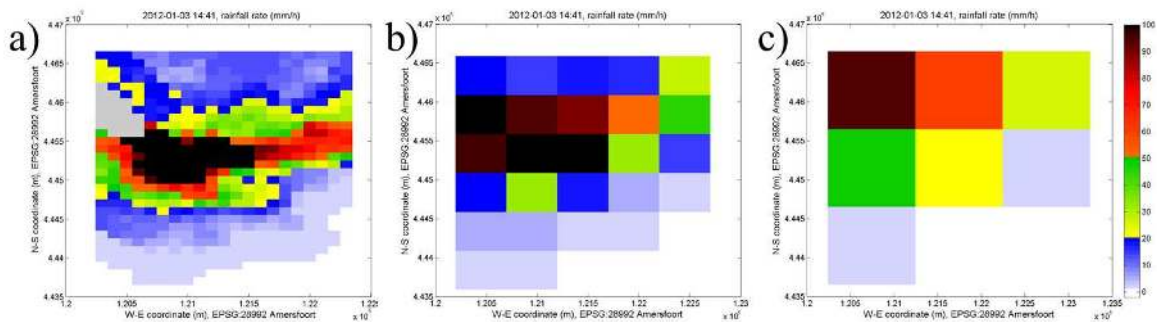

Figure 10: Rainfall rate over the catchment area for distinct spatial resolutions at 1441 UTC. Rainfall rate values over grid sizes of 100 by 100, 500 by 500, and 1000 by 1000 m are shown in panels a), b), and c), respectively. Note that high rainfall rate values decrease as the spatial resolution decreases.
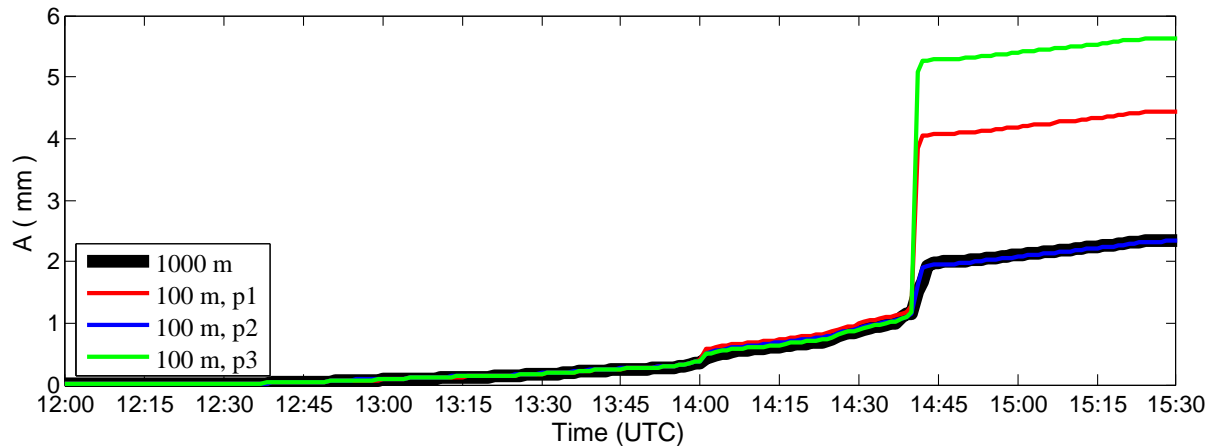
Figure 11: Accumulated rainfall depth from 1200 to 1530 UTC. Three grids of 100 by 100 m (p1, p2, and p3) are located inside of a bigger grid of 1000 by 1000 m (P). A from p1, p2, and p3 are depicted by the red, blue, and green lines, respectively. For grid P, A is shown by the thick black line. Note the variability on A shown by p1, p2, and p3.

national radar network. in 5th *European Conference of Radar Meteorology and Hydrology*, Helsinki, Finland.

Bluestein, H., 2008: On the decay of supercells through a "downscale transition": Visual documentation. *Monthly Weather Review*, **136**, 4013–4028.

Bringi, V. N., and V. Chandrasekar, 2001: *Polarimetric Doppler Weather Radar Principles and Applications*. Cambridge University Press, Cambridge, UK.

Brotzge, J. A., K. Brewster, B. Johnson, B. Philip, M. Preston, D. Westbrook, and M. Zink, 2005: CASA's first test bed: Integrative project #1. in 32nd *Conference on Radar Meteorology*, [Available online at http://ams.confex.com/ams/pdfpapers/97188.pdf]. Albuquerque, NM, Amer. Meteor. Soc., 14R.2.

Bruni, G., R. Reinoso-Rondinel, H. Russchenberg, and M.-C. ten Veldhuis, 2013: The use of x-band polarimetric radar to assess the impact of different temporal and spatial resolution on a drainage system in rotterdam urban area. in 11th *International Precipitation Conference*, Ede-Wageningen, The Netherlands.

Bunkers, M., M. Hjelmfelt, and P. Smith, 2006: An obsevational examination of long-lived supercells. part i: Characteristics, evolution, and demise. *Weather and Forecasting*, **21**, 673–688.

Doviak, R. J., and D. S. Zrnić, 1993: *Doppler Radar and Weather Observations*. Academic, San Diego, Calif.

Heijnen, S., L. Ligthart, and H. Russchenberg, 2000: First measurement with TARA: An s-band trans-

portable atmopsheric radar. *Phys. Chem. Earth*, **25**, 995–998.

i Ventura, J. F., and H. W. Russchenberg, 2009: Towards a better understanding of the impact of anthropogenic aerosols in the hydrological cycle: Idra, {IRCTR} drizzle radar. *Physics and Chemistry of the Earth, Parts A/B/C*, **34**(12), 88 − 92, ¡ce:title¿Sustainable Water Solutions¡/ce:title¿.

Lamb, D., and J. Verlinde, 2011: *Physics and Chemistry of Clouds*. Cambridge University Press, New York, USA.

Leijnse, H., R. Uijlenhoet, C. van de Beek, A. Overeem, T. Otto, C. Unal, Y. Dufournet, H. Russchenberg, J. F. I. Ventura, H. K. Baltink, and I. Holleman, 2010: Precipitation measurement at CESAR, the netherlands. *Journal of Hydrometeorology*, **11**, 1322–1329.

Maki, M., T. Maesaka, A. Kato, S. Shimizu, D.-S. Kim, K. Iwanami, S. Tsuchiya, T. Kato, Y. Kikumori, and K. Kieda, 2010: X-band polarimetric radar networks in urban areas. in *The 6th European Conference on Radar in Meteorology and Hydrology*.

Otto, T., and H. Russchenberg, 2012: Rainfall rate retrieval with IDRA, the polarimetric x-band radar at cabauw, netherlands. in *ERAD 2012: The 7th European Conference on Radar Meteorology and Hydrology*.

Schellart, A., W. Shepherd, and A. Saul, 2012: Influence of rainfall estimation error and spatial variability on sewer flow prediction at a small urban scale. *Advances in Water Resources*, **45**, 65–75.

Schuurmans, J., M. Bierkens, E. Pebesma, and R. Uijlenhoet, 2007: Autmatic predicition of high-resoltuion daily rainfall fields for multiple extends: the potential of operational radar. *Journal of Hydrometeorology*, **8**, 1204–1224.

Storm, B., M. Parker, and D. Jorgensen, 2007: A convective line with leading stratiform precipitation from BAMEX. *Monthly Weather Review*, **135**, 1769–1785.

Weisman, M., 2003: {CONVECTIVE} {STORMS} — overview. in E. in Chief:James R. Holton, editor, *Encyclopedia of Atmospheric Sciences*, pp. 548 – 559. Academic Press, Oxford.

Weisman, M., and R. Rotunno, 2004: "a theory for strong long-lived squall lines" revisited. *Journal of the Atmospheric Sciences*, **61**(4), 361–382.